Polarization-Modulated FTIR Spectroscopy of Lipid/Gramicidin Monolayers at the Air/Water Interface

Wolf-Peter Ulrich and Horst Vogel
Laboratoire de Chimie Physique des Polymères et Membranes, École Polytechnique Fédérale de Lausanne, CH-1015 Lausanne, Switzerland

ABSTRACT Monolayers of gramicidin A, pure and in mixtures with dimyristoylphosphatidylcholine (DMPC), were studied in situ at the air/H_2O and air/D_2O interfaces by polarization-modulated infrared reflection absorption spectroscopy (PM-IRRAS). Simulations of the entire set of amide I absorption modes were also performed, using complete parameter sets for different conformations based on published normal mode calculations. The structure of gramicidin A in the DMPC monolayer could clearly be assigned to a $\beta^{6.3}$ helix. Quantitative analysis of the amide I bands revealed that film pressures of up to 25–30 mN/m the helix tilt angle from the vertical in the pure gramicidin A layer exceeded 60°. A marked dependence of the peptide orientation on the applied surface pressure was observed for the mixed lipid-peptide monolayers. At low pressure the helix lay flat on the surface, whereas at high pressures the helix was oriented almost parallel to the surface normal.

INTRODUCTION

Amphipathic peptides are promising candidates for the design of surfaces with well-defined properties. In particular, their enormous potential for forming self-organized monomolecular layers with a large variety of possible structures opens a challenging field in surface engineering. Among these structures are not only α-helical and β-strand structures, which are ubiquitous in biology, but also tailor-made structures like nanotubes (Ghadiri et al., 1994) and template-assembled peptides (TASPs) (Tuchscherer and Mutter, 1995). The assembly of the individual peptide molecules as a monolayer typically takes place at an appropriate interface (gas/solid, gas/liquid, or liquid/liquid) that serves as primary ordering template. The first successful attempts have been undertaken (Boncheva and Vogel, 1997; Kim et al., 1998), but for a rational design of peptide monolayers, a deeper understanding of their self-assembly principles is required. An attractive and simple possibility for manipulating the self-organization process is to control the surface pressure of a monolayer at the gas/liquid interface by Langmuir techniques. Indeed, the surface pressure behavior of various peptides is being intensively investigated, and many, partly contradictory attempts have been made to obtain structural information from these experiments. Surprisingly, relatively few studies deal with the direct determination of molecular conformation and orientation at the air/water interface. Besides x-ray and neutron reflection techniques (Berge et al., 1998; Lu and Thomas, 1998; Majewski et al., 1998; Naumann et al., 1996), one of the most promising approaches is infrared reflection absorption spectroscopy (Cornut et al., 1996; Flach et al., 1997; Gericke et al., 1997). However, in the latter case the problem of omnipresent and very strong water vapor bands must be overcome. These bands cover the spectral region of 1300–2000 cm^{-1}, which also contains essential structural information originating from the amide I, amide II, carbonyl stretching, and methylene bending modes. An elegant way to overcome this problem is to selectively detect surface species by differential spectroscopy. This can be achieved by polarization modulation (PM) of the infrared light. This technique was originally developed for solid surfaces and has been successfully adopted to the spectroscopic characterization of molecules at the air/water interface within the last decade (Buffeteau et al., 1991; Blaudez et al., 1993, 1994, 1996; Cornut et al., 1996).

The present work concentrates on the orientation and conformation of gramicidin A at the air/water interface. Gramicidin A is a linear pentadecapeptide of alternating L- and D-amino acids (Sarges and Witkop, 1965) from *Bacillus brevis* that forms ion-selective membrane channels: formyl-L-X-Gly-L-Ala-D-Leu-L-Ala-D-Val-L-Val-D-Val-L-Trp-D-Leu-L-Trp-D-Leu-L-Trp-ethanolamine. Gramicidin adopts different conformations, depending on the environment and the pretreatment (Wallace, 1998). In lipid bilayers it is well established that it takes up a single-stranded $\beta^{6.3}$ structure (Ketchem et al., 1993, 1997; Wallace, 1992; Nabedryk et al., 1982; Urry, 1971). In contrast, in solution and in crystalline form, several different structures of intertwined helical dimers have been reported. Among them are antiparallel strands of $\beta^{5.6}$ helices (Langs, 1988) and $\beta^{7.2}$ helices (Wallace and Ravikumar, 1988), the latter as a cesium complex.

Here we present polarization-modulated infrared spectra of monolayers of pure gramicidin A as well as of mixtures with DMPC at the air/water interface. The experiments are complemented by simulations of polarization-modulated infrared spectra based on a well-established optical model (Yamamoto and Ishida, 1994; Mendelsohn et al., 1995).

Received for publication 10 September 1998 and in final form 14 December 1998.

Address reprint requests to Dr. Horst Vogel, Laboratoire de Chimie Physique des Polymères et Membranes, École Polytechnique Fédérale de Lausanne, CH-1015 Lausanne, Switzerland. Tel.: 41-21-6933155; Fax: 41-21-6936190; E-mail: horst.vogel@epfl.ch.

0006-3495/99/03/1639/09 $2.00

Recently, the strength of this approach has been evaluated thoroughly (Flach et al., 1997). To derive reliable information on the orientation of the peptide helix in the monolayer from the infrared (IR) spectra, it is crucial to know the direction of the transition dipole moment of the amide I band. More precisely, amide I bands typically comprise several modes that have to be taken into account, if they are of considerable intensity. In this work we address this problem by calculating PM-IRRAS spectra based on the normal mode calculations of Naik and Krimm (1986a), which provide a complete description of amide I bands for all possible conformations of gramicidin A.

MATERIALS AND METHODS

Gramicidin A was purchased from Fluka (Buchs, Switzerland). Dimyristoylphosphatidylcholine (DMPC) was obtained from Avanti Polar Lipids (Alabaster, AL). Water was purified with a MilliQ purification system and had a resistivity higher than 18 MΩ cm. Deuterium oxide (D_2O) with 99.8% isotopic enrichment was supplied by Reactolab (Servion, Switzerland). High-performance liquid chromatography-grade methanol and chloroform were purchased from Fluka (Switzerland).

Gramicidin A, DMPC, and a 1:8 molar ratio mixture of the two were dissolved in methanol/$CHCl_3$ (1:1) to a final overall concentration of 1 mg/ml.

Pressure-area isotherms as well as PM-IRRAS measurements on H_2O as a subphase were carried out on a commercial film balance (Riegler and Kirstein, Berlin, Germany). Monolayers were formed by depositing a small amount of the solution on the surface of the water with a microliter syringe and allowing the solvent to evaporate. All measurements were performed at a temperature of 20°C. Experiments with D_2O were performed on a homemade miniaturized trough milled from Teflon with a subphase volume of only 10 ml. Because of the miniaturization, this trough had no facility for adjusting the surface area. Therefore, films were directly spread to the appropriate film pressure. For both troughs the film pressure was measured by the Wilhelmy plate method. The D_2O trough was enclosed in a plexiglass chamber (5 × 5 × 15 cm). The gas-tight chamber could be connected to two tubes sealed with BaF_2 windows, which led to the photoelastic modulator (PEM) and the ZnSe lens, respectively. Before spectra were acquired, this assembly was purged overnight with dry nitrogen. Then the trough was filled with D_2O with a syringe through a septum located on top of the plexiglass chamber. These measures were taken to keep the exchange of D_2O with H_2O as low as possible. Before film spreading, background spectra of the pure subphase were recorded.

PM-IRRAS spectra were recorded on a Vector 22 Spectrometer (Bruker, Karlsruhe, Germany) equipped with an external polarization modulation set-up (Fig. 1). The efficiency of the polarizer was specified as ranging from 98.2% (3000 cm^{-1}) to 99.5% (1000 cm^{-1}). The chosen angle of incidence was 75°, with an accuracy of ±1°. The photoelastic modulator (PEM-90; Hinds Instruments, Hillsboro, OR) modulated the polarization of the infrared light at a frequency of 74 kHz. Demodulation was performed with a lock-in amplifier (Princeton Applied Research, model 5209) and a low-pass filter (Stanford Research SR650). The optical velocity of the interferometer mirror was set at 0.47 cm/s. A total of 2000–5000 scans were recorded at 4 cm^{-1} resolution. Spectra were apodized with a triangular function and Fourier transformed with one level of zero filling. None of the spectra were smoothed.

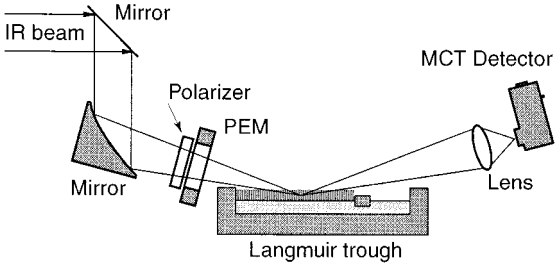

FIGURE 1 Scheme of the PM-IRRAS set-up. The optical pathway encloses several plane mirrors, one off-axis parabolic mirror, a BaF_2 wire grid polarizer, a photoelastic modulator, a ZnSe lens, and a MCT detector.

The principle of PM-IRRAS reflection absorption spectroscopy has already been described in detail elsewhere (Golden, 1985; Buffeteau et al., 1991; Hipps and Crosby, 1979). The measurable quantity, i.e., the polarization-modulated reflectivity S, is given as the ratio of the difference and the sum signal:

$$S = C\frac{J_2(\phi_0)(R_p - R_s)}{(R_p + R_s) + J_0(\phi_0)(R_p - R_s)},$$

where R_p and R_s are the reflectivities for polarization parallel and perpendicular to the plane of incidence and c is the electrical amplification ratio of the two signals. J_2 and J_0 are the second- and zero-order Bessel functions of the maximum dephasing angle ϕ_0 that is introduced by the PEM. Spectral data are represented as

$$\frac{S - S_0}{S_0},$$

where S and S_0 are the PM-IRRAS signals of the film-covered and film-free surface, respectively. This representation is independent of J_2 and C and reduces the large signal from the dielectric subphase. The resulting spectra can contain positive as well as negative bands, depending on the angle of incidence and the orientation of the transition moments. At the given angle of incidence of 75°, a positive reflection absorption band indicates a transition moment oriented preferentially in the plane of the surface, whereas a negative band indicates a transition moment oriented preferentially perpendicular to the surface. Intermediate transition moments give rise to a band with adjacent positive and negative components.

Simulation of spectra was performed using a self-developed computer program that computes the Fresnel reflection coefficients for parallel and perpendicular polarized light. There are several approaches described in the literature (Mendelsohn et al., 1995) that give virtually the same results. We implemented the one developed by Yamamoto and Ishida (1994). It is easily programmable and offers great flexibility because there are no restrictions concerning the number of layers. The mathematical formalism is based on the matrix method of Abelès (Born and Wolf, 1980), which describes stratified layers of homogeneous films. Appropriate modifications to account for absorbing (Dluhy, 1986; Hansen, 1968) and anisotropic (Yamamoto and Ishida, 1994) layers are included.

The final algorithm is valid for any system of stratified layers of absorbing, anisotropic, homogeneous material between a transparent semiinfinite incident medium and an absorbing, anisotropic, homogeneous, semiinfinite substrate.

Because the theory has been fully presented elsewhere (Yamamoto and Ishida, 1994), in the following description only the equations relevant to the computer program are summarized. Fig. 2 *a* gives a physical description on the basis of a three-phase system. The optical properties of the jth phase of the system are described by the anisotropic complex refractive indices in the c direction, where c represents x, y, or z coordinates:

$$\hat{n}_{jc} = n_{jc} + ik_{jc}.$$

The characteristic matrices of the jth layer are defined as follows:

$$M_j = \begin{bmatrix} \cos\beta_{jl} & \frac{-i}{g_{jl}}\sin\beta_{jl} \\ -ig_{jl}\sin\beta_{jl} & \cos\beta_{jl} \end{bmatrix},$$

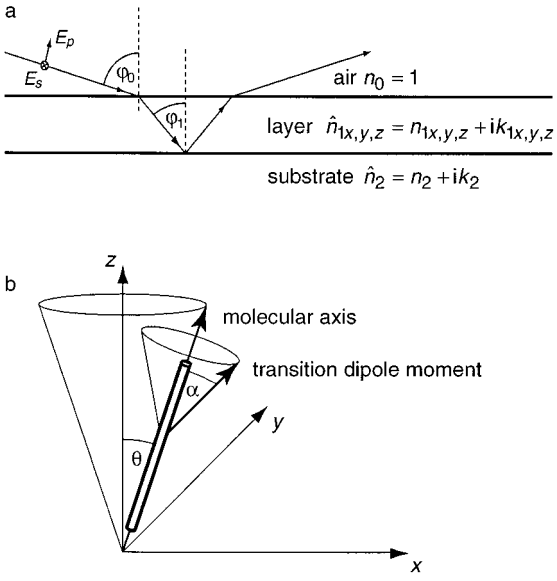

FIGURE 2 (*a*) Schematic illustration of the optical model of a three-phase system. (*b*) Definition of the coordinate system. The rotational freedom of motion of the peptide around the *z* axis and of the transition moment around the molecular axis is shown. Symbols are described in the text.

where *l* represents perpendicular (s) or parallel (p) polarization and

$$\beta_{js} = 2\pi \frac{d_j}{\lambda} \hat{n}_{jy} \cos \hat{\varphi}_{js}, \quad \beta_{jp} = 2\pi \frac{d_j}{\lambda} \hat{n}_{jx} \cos \hat{\varphi}'_{jp},$$

and

$$g_{js} = \hat{n}_{jy} \cos \hat{\varphi}_{js}, \quad g_{jp} = \frac{\cos \hat{\varphi}'_{jp}}{\hat{n}_{jx}},$$

with

$$\hat{n}_0 \sin \hat{\varphi}_0 = \hat{n}_{jy} \sin \hat{\varphi}_{js}, \quad \hat{n}_0 \sin \hat{\varphi}_0 = \hat{n}_{jz} \sin \hat{\varphi}'_{jp}.$$

d_j represents the thickness and $\hat{\varphi}_{jl}$ the complex refractive angle of the *j*th layer. For an *N*-phase system ($0 \le j \le N - 1$) the overall matrix of the stratified layers results in

$$\mathbf{M} = \sum_{j=1}^{N-2} M_j.$$

The reflection coefficients may be derived from the elements m_{ik} of the matrix

$$\mathbf{M} = \begin{bmatrix} m_{11} & m_{12} \\ m_{21} & m_{22} \end{bmatrix}$$

as

$$\hat{r}_l = \frac{(m_{11} + m_{12} g_{(N-1)l}) g_{0l} - (m_{21} + m_{22} g_{(N-1)l})}{(m_{11} + m_{12} g_{(N-1)l}) g_{0l} + (m_{21} + m_{22} g_{(N-1)l})}.$$

The reflectivities of the film-free, R_l^0, and film-covered, R_l, surfaces for parallel (l = p) and perpendicular (l = s) polarized light are calculated from the reflection coefficients using

$$R_l^0 = \hat{r}_l^0 \hat{r}_l^{0*}$$

and

$$R_l = \hat{r}_l \hat{r}_l^*.$$

To perform the simulation, values for $\hat{n}_{jc}$ must be found. The directional extinction coefficients $k_{x\,max}$, $k_{y\,max}$, and $k_{z\,max}$ of an anisotropic layer can be determined from the transition dipole strength k_{max}. Therefore the orientational distribution of the tilt angle, $\langle\theta\rangle$, between the main molecular axis and the surface normal (*z* axis) must be taken into account. Furthermore, assuming the transition dipolar moments to be equally distributed around the molecular axis at an orientational distribution $\langle\alpha\rangle$ (Fig. 2 *b*), the formalism of Fraser and MacRae (1973) for uniaxial symmetry in protein fibers applies:

$$k_{x\,max} = k_{y\,max} = [\tfrac{1}{2}\langle \sin^2\alpha \rangle + \tfrac{1}{3}(1 - f)] k_{max},$$

and

$$k_{z\,max} = [\langle \cos^2\alpha \rangle + \tfrac{1}{3}(1 - f)] k_{max},$$

with the orientational distribution order parameter

$$f = \tfrac{1}{2}(3\langle \cos^2\theta \rangle - 1),$$

where $\langle\alpha\rangle$ and $\langle\theta\rangle$ reflect conformational fluctuations in the peptide and orientational fluctuations of the peptide in the monolayer, respectively. However, the orientational density functions that determine these distributions are unknown. In our calculations, we chose Dirac functions to describe the orientational density functions, resulting in $\theta = \langle\theta\rangle$ and $\alpha = \langle\alpha\rangle$.

The whole absorption band is expressed as an antisymmetrical linear combination of two Lorentzian functions (Ohta and Ishida, 1988):

$$k_c(\tilde{\nu}) = \frac{k_{c\,max}(\text{fwhh}/2)^2}{(\tilde{\nu} - \tilde{\nu}_0)^2 + (\text{fwhh}/2)^2} - \frac{k_{c\,max}(\text{fwhh}/2)^2}{(\tilde{\nu} + \tilde{\nu}_0)^2 + (\text{fwhh}/2)^2},$$

where fwhh is the full width at half-height, $\tilde{\nu}_0$ is the center wavenumber of the absorption band, $\tilde{\nu}$ is the actual wavenumber, and c represents x, y, z coordinates. The corresponding relations for the real refractive indices result from the Kramers-Kronig transformation of the last equation:

$$n_c(\tilde{\nu}) = n_c^\infty - \frac{k_{c\,max}(\tilde{\nu} - \tilde{\nu}_0)(\text{fwhh}/2)}{(\tilde{\nu} - \tilde{\nu}_0)^2 + (\text{fwhh}/2)^2} + \frac{k_{c\,max}(\tilde{\nu} + \tilde{\nu}_0)(\text{fwhh}/2)}{(\tilde{\nu} + \tilde{\nu}_0)^2 + (\text{fwhh}/2)^2},$$

where n_c^∞ is the constant refractive index in the near-infrared.

The angles α of the transition dipolar moments for amide I modes of the previously described structures of gramicidin A were derived from normal mode calculations (Naik and Krimm, 1986a). The results are shown in Table 1. The actual thickness of the gramicidin A layer was assumed to be between two limits defined by $d \approx 12.5$ Å for the $\beta^{6.3}$ helix lying flat on the surface and $d \approx 31$ Å for the $\beta^{5.6}$ helix standing upright. Hence, the thickness of the layer was far below the critical value where differences of the optical path due to reflection at the two interfaces come into play. Because, in this study, absorption is not considered in a quantitative manner, the absolute value of d as well as of the extinction coefficient k_{max} is not crucial. For the refractive index of the layers a value of $n_c^\infty = 1.41$ was chosen. Data for the complex refractive index of the H_2O or D_2O subphase were taken from the literature (Bertie et al., 1989) and extrapolated to the desired stepwidth.

TABLE 1 Relative intensities of amide I modes and angles of transition dipole moments, α, for $\beta^{6.3}$ and $\beta^{5.6}$ conformations of gramicidin A as derived from normal mode calculations (Naik and Krimm, 1986a)

Conformation	Wavenumber* (cm^{-1})	Relative intensity	α (°)
$\beta^{6.3}$	1652	0.467	57.8
	1643	1.036	10.8
	1654	0.0802	87.1
	1645	0.007	80.1
$\beta^{5.6}$	1672	0.073	78.3
	1669	0.267	7.8
	1666	0.370	8.2
	1636	2.507	50.8
	1675	0.475	84.7
	1669	0.083	77.3
	1666	0.084	77.4
	1656	0.007	50.4

* Accuracy of wavenumber prediction ± 5 cm^{-1}.

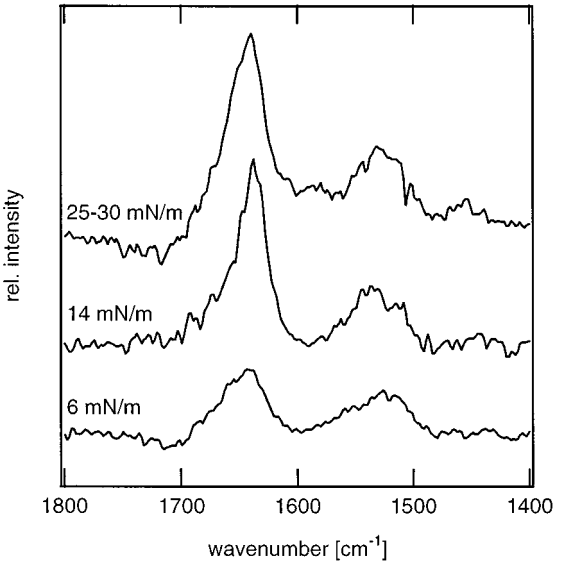

FIGURE 3 PM-IRRAS spectra of the spectral region 1800–1400 cm^{-1} of gramicidin A at the air/H_2O interface at the indicated film pressures.

RESULTS AND DISCUSSION

Monolayers of DMPC/gramicidin mixtures were prepared as described on the large as well as on the small Langmuir trough. DMPC and DMPC/gramicidin monolayers could easily be compressed or directly spread up to a lateral film pressure of 40 mN/m. No differences between the spectra were observed for the two spreading techniques. Thus in these cases the spreading procedure does not significantly influence structural features of the film that are detectable by IR spectroscopy.

Pure gramicidin layers

Pure gramicidin layers were typically examined at lower surface pressures, mainly for two reasons. First, gramicidin films at higher surface pressure are known to be extremely stiff, and the Wilhelmy plate tends to be pushed out of the subphase (Ducharme et al., 1996). Under these conditions the lateral film pressure cannot be measured precisely. Second, it is doubtful whether such rigid films could be produced by the direct spreading procedure due to the likely formation of collapse-like structures. However, on H_2O subphases we compressed gramicidin films to higher film pressures. The film was compressed to an area per molecule that was known to give the desired film pressure. The corresponding pressure-area isotherms made with a Langmuir-type measuring system were taken from the literature (Ducharme et al., 1996).

In Fig. 3, spectra of gramicidin on an H_2O subphase at three different film pressures, π, are shown. For $\pi = 14$ mN/m and $\pi = 25$–30 mN/m, the amide I band is located at 1636–1638 cm^{-1}, the amide II band at 1533–1535 cm^{-1}. For $\pi = 6$ mN/m, the amide I band is shifted to slightly higher and the amide II band to slightly lower wavenumbers. Because of the very broad bands and the limited S/N ratio, a more precise determination of the wavenumbers is ambiguous.

Based on these data, it is not possible to distinguish between the $\beta^{6.3}$ and $\beta^{5.6}$ helices from the location of the amide I band. Although a small difference in wavenumbers of the main peak is predicted from the normal mode calculations (Table 1) (Naik and Krimm, 1986a), experimental data gave a value of 1638 cm^{-1} for both structures (Naik and Krimm, 1986b; Nabedryk et al., 1982). The asymmetry of the measured amide I bands indicates the presence of a second component. We were not able to resolve this band precisely enough to decide whether its maximum is located at ~1650 cm^{-1} ($\beta^{6.3}$ helix) or ~1670 cm^{-1} ($\beta^{5.6}$ helix).

Experimental values for the amide II band have been found to be 1547 cm^{-1} for the $\beta^{6.3}$ helix (Nabedryk et al., 1982) and 1542 cm^{-1} for the $\beta^{5.6}$ helix (Naik and Krimm, 1986b), respectively. Neither of these values fits well with our findings, even though the agreement is better for the $\beta^{5.6}$ helix.

To elucidate the influence of the orientation of gramicidin within the layer on the amide I band, two sets of simulations were performed for the $\beta^{5.6}$ helix and the $\beta^{6.3}$ helix, respectively. The simulations are based on the values given in Table 1. The results are displayed for different tilt angles from 0° to 90° (Fig. 4).

At a tilt angle of 90°, the spectra for both conformations are dominated by a single positive peak near 1640 cm^{-1}. At lower tilt angles, the positive peak diminishes and a negative peak occurs. In the case of the $\beta^{6.3}$ helix, the positive peak vanishes completely and the negative peak appears at slightly higher wavenumbers. This result is in qualitative agreement with that obtained for the simulation of an α-helix (Cornut et al., 1996), which is not surprising, because the angles of the main mode transition moments of 11° or 28°, respectively, are quite similar. In the case of the $\beta^{5.6}$ helix, the positive peak diminishes only moderately and the negative peak arises at much higher wavenumbers. From a

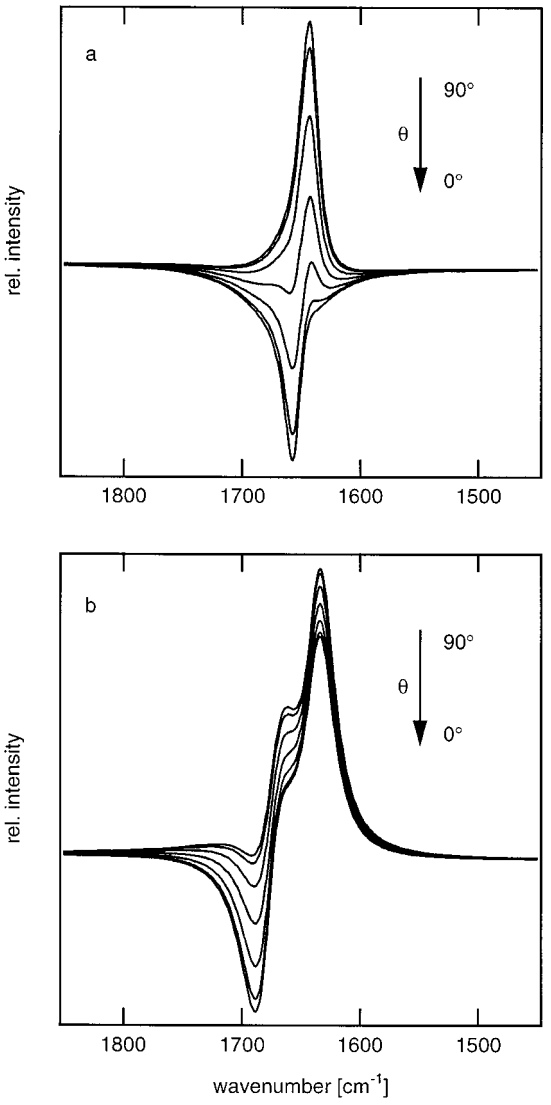

FIGURE 4 Simulated PM-IRRAS spectra of the amide I band of gramicidin A at the air/H_2O interface for tilt angles from $\theta = 90°$ to $\theta = 0°$ in steps of 15°. The refractive index of the film was $n_1 = 1.41$. Other parameters were taken from Table 1. (*a*) Spectra for the $\beta^{6.3}$ conformation. (*b*) Spectra for $\beta^{5.6}$ conformation.

comparison of the measured and simulated spectra, two conclusions can be drawn. First, with the present data it is not possible to clearly distinguish between $\beta^{5.6}$ and $\beta^{6.3}$ helices. Second, irrespective of the conformation, at $\pi =$ 25–30 mN/m the tilt angle θ of the gramicidin helix exceeds 60°.

Mixed DMPC/gramicidin layers

Fig. 5 displays the spectral region between 1800 and 1400 cm^{-1} for pure DMPC layers at 30 mN/m (Fig. 5 *a*), pure gramicidin layers at 14 mN/m (Fig. 5 *b*), and the DMPC/gramicidin mixture at 30 mN/m (Fig. 5 *c*), each on an H_2O subphase. The carbonyl stretching vibration at ~1733 cm^{-1}, as well as the methylene scissoring vibration at

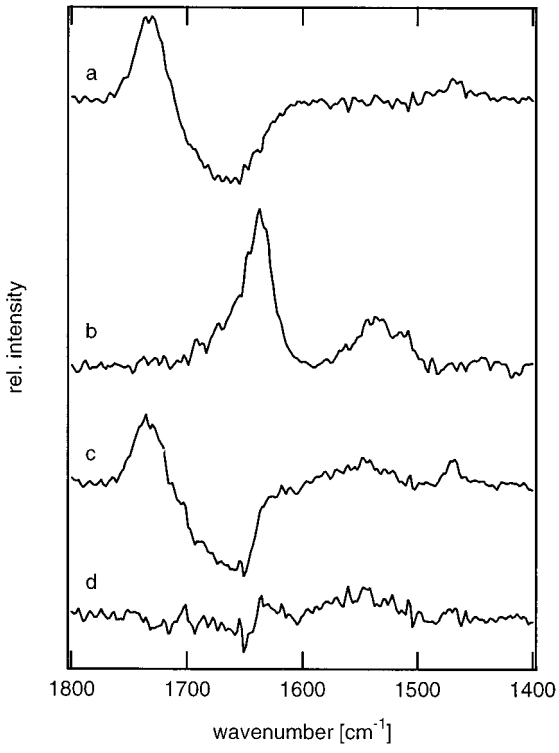

FIGURE 5 PM-IRRAS spectra taken at the air/H_2O interface of (*a*) a pure DMPC monolayer at 30 mN/m, (*b*) a pure gramicidin layer at 14 mN/m, (*c*) a DMPC/gramicidin A layer (8:1 molar ratio), and (*d*) weighted subtraction of spectrum *a* from spectrum *c* to eliminate $\delta(H_2O)$.

~1468 cm^{-1}, of the lipid are clearly visible in spectra *a* and *c*. The spectrum of the pure gramicidin layer (Fig. 5 *b*) has already been described in the last section. It shows the amide I mode at ~1636 cm^{-1} and the amide II at ~1535 cm^{-1}. The broad negative band in *a* and *c* at 1660 cm^{-1} stems from the $\delta(H_2O)$ bending mode of the liquid water subphase. Note that the spectrum of the pure gramicidin layer also contains a superimposition of the amide I band and the $\delta(H_2O)$ mode, although the latter is completely hidden by the amide band. The spectral region where the amide I band of the mixed layer (Fig. 5 *c*) is supposed to be located is completely dominated by the $\delta(H_2O)$ mode. Apparently, the intensity of the gramicidin amide I band is rather low. This is due to the following: 1) The gramicidin content in the mixed layer is only 11 mol%. 2) From Fig. 4, the intensity is also strongly dependent on the orientation of the helix.

At a first glance it may seem surprising that the spectral absorption of the putatively isotropic bulk water subphase is not eliminated by the polarization modulation. However, at and near the surface, the mean square electric field intensities in the *x* and *y* directions are reduced compared to the *z* direction because of interference between incident and reflected light (Dluhy, 1986), which implies a difference in absorption of parallel and perpendicular polarization. However, experimental $\delta(H_2O)$ bands show a considerably higher intensity than simulations that take account of this

problem. Consequently, this spectral feature cannot be fully attributed to a difference in reflectivity between covered and uncovered water surfaces. The origin of this apparent discrepancy between experiment and simulation has been explained as being due to a thin layer of oriented water molecules beneath the surface layer (Blaudez et al., 1996). The properties of this water layer will strongly depend on the physical state and the chemical composition of the monolayer. The $\delta(H_2O)$ mode for the mixed DMPC/gramicidin layer might differ from that for the pure DMPC layer in both intensity and wavenumber. Consequently, it is not straightforward to extract the low-intensity amide I band signal in the mixed layer from the large water band. Nevertheless, the subtraction of the DMPC spectrum from the DMPC/gramicidin spectrum was carried out, and in such a way as to ensure complete elimination of the DMPC carbonyl stretching band. The resulting difference spectrum is shown in Fig. 5 *d*. A signal—apparently consisting of a positive and a negative component—appears in the region where the amide I band of gramicidin should be found. However, artifacts may arise from the subtraction procedure, and the noise of the spectrum is substantially increased. For these reasons this signal could not be unambiguously assigned to the amide I band.

Therefore, to facilitate the interpretation of the spectra of mixed DMPC/gramicidin monolayers, the same measurements were performed on D_2O subphases. In these measurements the $\delta(H_2O)$ mode disappears and is replaced by the $\delta(D_2O)$ mode located near 1200 cm^{-1}. In Fig. 6 the spectral region between 1800 and 1400 cm^{-1} is depicted for DMPC (Fig. 6 *a*), gramicidin (Fig. 6 *b*), and the DMPC/gramicidin mixture (Fig. 6 *c*) for D_2O subphases. As expected, the position of the C=O stretching band in Fig. 6 *a* does not change significantly. The $\delta(H_2O)$ mode has vanished completely in spectra *a* and *c*. The very strong and broad band below 1500 cm^{-1} (Fig. 6, *a–c*) is mainly caused by the δ(HOD) mode. Hydrogen most probably originates as traces of H_2O that accumulate with time in the D_2O subphase.

The amide I band of gramicidin (Fig. 6 *b*) is now located at ~1630 cm^{-1}. It is shifted by 6 cm^{-1} to lower wavenumbers, as previously reported by other authors (Naik and Krimm, 1986b). The amide II band is shifted, because of the H-D exchange of the amide bond, to the region that is covered by the δ(HOD) mode.

Because the complex refractive index of D_2O differs from that of H_2O, the intensities of the bands for the two subphases are also different. In the wavenumber range under consideration, the bands for D_2O subphases are weaker than those for H_2O subphases. The C=O stretching band of DMPC is of ~20–25% lower intensity (peak height) on D_2O than on H_2O, which is in good agreement with our simulations (20%). In contrast, the amide I band of the pure gramicidin layer is ~20% stronger than on an H_2O subphase, which can be attributed to the overlap of the amide I band on H_2O subphases with the negative $\delta(H_2O)$ mode. This compares well with simulations of the amide I band for D_2O subphases, which predict increases in intensity of 22% ($\beta^{6.3}$ helix) and 25% ($\beta^{5.6}$ helix). It implies that for the pure gramicidin layer the $\delta(H_2O)$ mode is as large as expected from the simulations.

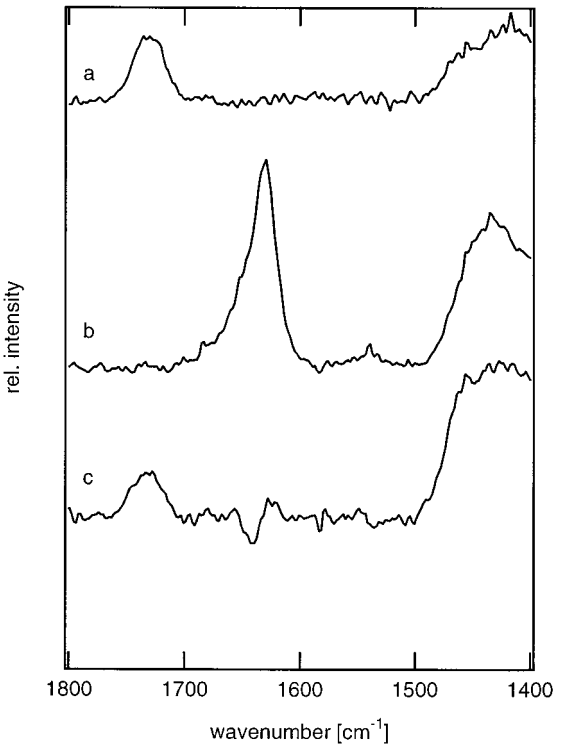

FIGURE 6 PM-IRRAS spectra at the air/D_2O interface of (*a*) a pure DMPC layer at 30 mN/m, (*b*) a pure gramicidin layer at 14 mN/m, (*c*) a DMPC/gramicidin A layer (8:1 molar ratio).

In the spectrum of the mixed DMPC/gramicidin layer (Fig. 6 *c*), a band arises at ~1640 cm^{-1}. This band can only be assigned to the amide I mode of gramicidin. Qualitatively, it coincides with the signal obtained from the difference spectrum for the H_2O subphase (Fig. 5 *d*). The signal-to-noise ratio is sufficient to allow a more quantitative analysis of the peak intensities. To do so, a series of spectra for DMPC/gramicidin monolayers were recorded at different film pressures in the range of 6–40 mN/m. The results are shown in Fig. 7 *a*. At low surface pressure the amide I modes of gramicidin form a positive absorption band. This band is rather broad, and its maximum occurs at ~1642 cm^{-1}. With increasing surface pressure the band sharpens and gains intensity, and the maximum shifts to ~1625 cm^{-1}. Subsequently, a negative band evolves at the expense of the positive band, resulting in an almost negative band at very high surface pressure.

As outlined in Materials and Methods, the positive absorption band at low surface pressure indicates a transition moment in the surface plane. Band shape and maximum are different from those obtained from pure gramicidin layers as well as from the mixed layers at higher surface pressures. This might be due to a different conformation of gramicidin at low surface pressures.

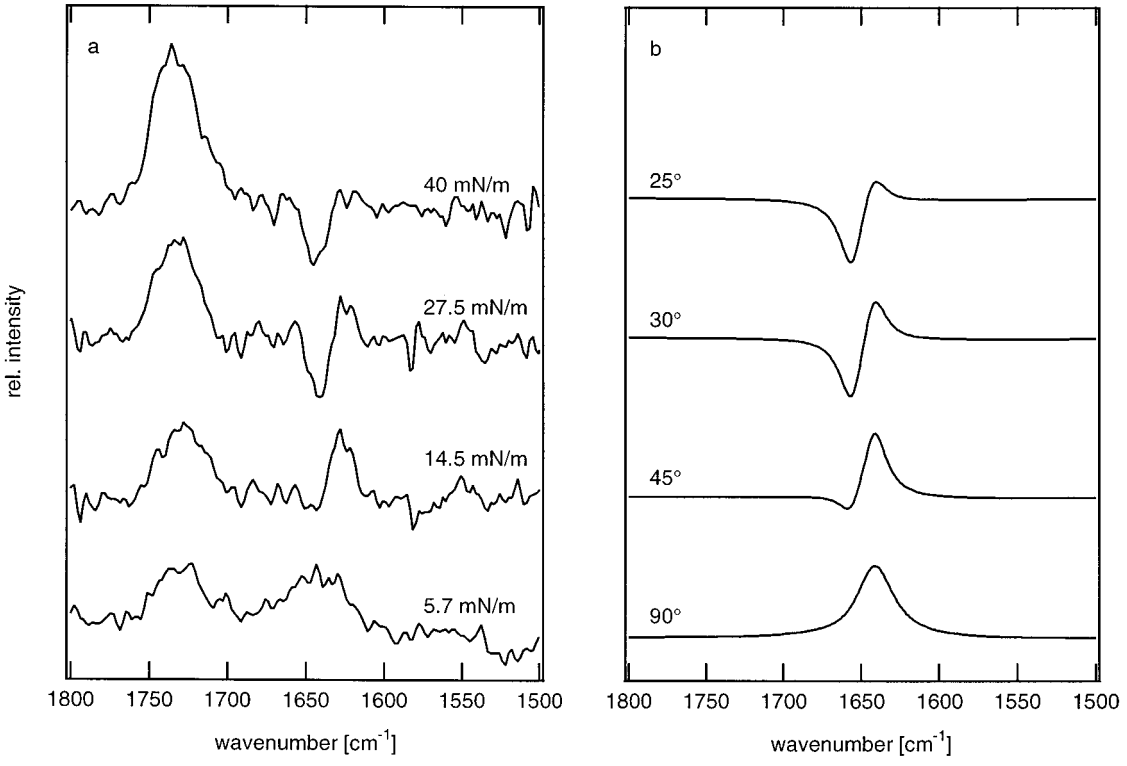

FIGURE 7 (*a*) PM-IRRAS spectra of a DMPC/gramicidin A layer (8:1 molar ratio) at the indicated film pressures on a D_2O subphase. (*b*) Simulated PM-IRRAS spectra of the amide I band of a DMPC/gramicidin A layer (8:1 molar ratio) at the indicated tilt angles, θ, on a D_2O subphase.

The formation of the negative band at higher surface pressure reveals that the orientation of the transition moment becomes increasingly perpendicular to the surface. To elucidate this point, we performed a series of simulations for the amide I band in the mixed layer for a variety of tilt angles of the peptide assuming $\beta^{6.3}$ conformation. The results of these simulations for the $\beta^{6.3}$ helix are presented in Fig. 7 *b*. A comparison of Fig. 7 *a* and Fig. 4 reveals that the $\beta^{5.6}$ conformation can be eliminated. It is clearly not consistent with the data. Neither the disappearance of the positive peak nor the appearance of the negative peak occurs at the correct wavenumber. The tilt angles in Fig. 7 *b* have been chosen to give the best fit to the measured spectra. The intensity of the simulated bands was scaled differently for each spectrum to reproduce the intensities of the measured bands reasonably well. A comparison of the measured and the simulated data clearly reveals the raising of the gramicidin helix upon compression.

A lipid monolayer with a surface pressure on the order of 30 mN/m represents the situation in a lipid bilayer (Jähnig, 1996). Therefore it is interesting to compare the tilt angle found for this particular film pressure with tilt angles found in lipid bilayers. With a refractive index of $n = 1.41$, we obtain a tilt angle of $31 \pm 5°$. The error was estimated on the basis of several measurements and takes account of the uncertainty in determining the ratio of positive and negative band components.

The tilt angle of $31 \pm 5°$ is higher than what has been determined for gramicidin incorporated in DMPC vesicles ($\theta = 15°$) (Nabedryk et al., 1982). However, at that time no structural data were available for the $\beta^{6.3}$ helix, so the authors chose the transition moments from the then available structure of the $\beta^{4.4}$ helix. For this structure the transition moment was known to form an angle of 22° with the helix axis. Using the correct angle, $\alpha = 10.8°$, we calculate from their data a tilt angle of 25°, which is in good agreement with our data.

The reliability of the tilt angle predictions presented here depends strongly on the tilt angle itself. For tilt angles $\theta > 60°$, the band consists of one single positive peak. In this situation the only measure of the tilt angle is the peak intensity. However, the intensity also depends on the absorption coefficient, the film thickness, and the surface coverage. Taking these additional factors into account introduces additional errors. In contrast, for $15° < \theta < 50°$, taking the ratio of the intensities of the positive and negative components of the band, I_+ and I_-, eliminates the dependence on absolute intensities. In Fig. 8 the dependence of the ratio $D_{PM} = |I_+/I_-|$ on θ is shown. Similar graphs facilitating the determination of tilt angles from D_{PM} can be set up for different peptide conformations if α and n of the layer are known. However, one has to be aware of the fact that uncertainties in the estimation of refractive indices of the film and in the normal mode calculations might strongly

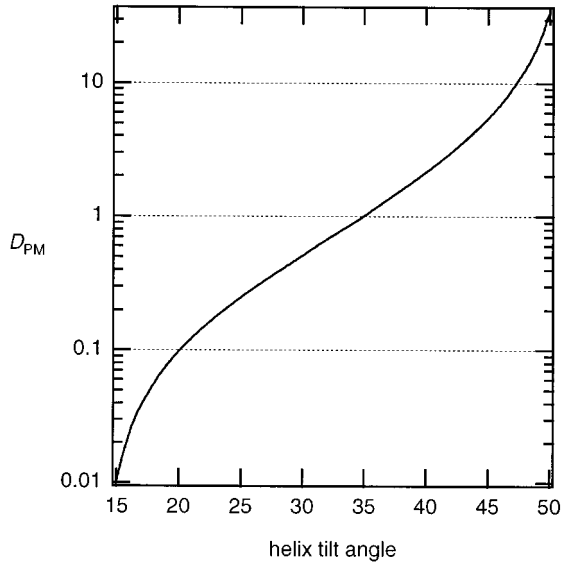

FIGURE 8 The ratio D_{PM} of the positive and negative components of the PM-IRRAS spectra as a function of the tilt angle, θ, for the $\beta^{6.3}$ conformation of gramicidin.

affect the resulting tilt angle of the helix (Axelsen et al., 1995).

CONCLUSIONS

PM-IRRAS in combination with simulations allowed us to study the conformation and orientation of gramicidin A at the air/water interface. If the angles of the contributing transition dipole moments with the molecular helix axis are known, the tilt angle of the helix at the water surface can be estimated from a single PM-IRRAS spectrum. In the present work the dipole moments could be derived from normal mode calculations. Within the applied pressure regime, the orientation of the pure peptide film seems to be only moderately dependent on the lateral pressure. In contrast, if the peptide is confined to a lipid monolayer, the orientation depends strongly on the lateral pressure, suggesting an alignment of the helix along the lipid chains. In this case, the lipid can be used as a matrix to orient the peptide in the desired manner. PM-IRRAS at the air/water interface has been shown to be a valuable tool for determining structural details of peptides at interfaces. This may accelerate the development of novel surface layers that are based on such amphiphilic peptides.

REFERENCES

Axelsen, P. H., B. K. Kaufman, R. N. McElhaney, and R. N. A. H. Lewis. 1995. The infrared dichroism of transmembrane helical polypeptides. *Biophys. J.* 69:2770–2781.

Berge, B., P. F. Lenne, and A. Renault. 1998. X-ray grazing incidence diffraction on monolayers at the surface of water. *Curr. Opin. Colloid Interface Sci.* 3:321–326.

Bertie, J. E., M. K. Ahmed, and H. H. Eysel. 1989. Infrared intensities of liquids. 5. Optical and dielectric constants, integrated intensities, and dipole moment derivatives of H_2O and D_2O at 22°C. *J. Phys. Chem.* 93:2210–2218.

Blaudez, D., T. Buffeteau, J. C. Cornut, B. Desbat, N. Escafre, M. Pezolet, and J. M. Turlet. 1993. Polarization-modulated FT-IR spectroscopy of a spread monolayer at the air/water interface. *Appl. Spectrosc.* 47: 869–874.

Blaudez, D., T. Buffeteau, J. C. Cornut, B. Desbat, N. Escafre, M. Pezolet, and J. M. Turlet. 1994. Polarization-modulated FT-IR spectroscopy at the air/water interface. *Thin Solid Films.* 242:146–150.

Blaudez, D., J.-M. Turlet, J. Dufourcq, D. Bard, T. Buffeteau, and B. Desbat. 1996. Investigations at the air/water interface using polarization modulation IR spectroscopy. *J. Chem. Soc. Faraday Trans.* 92:525–530.

Boncheva, M., and H. Vogel. 1997. Formation of stable polypeptide monolayers at interfaces: controlling molecular conformation and orientation. *Biophys. J.* 73:1056–1072.

Born, M., and E. Wolf. 1980. Basic properties of the electromagnetic field. *In* Principles of Optics, 6th Ed. Pergamon Press, Oxford. 1–70.

Buffeteau, T., B. Desbat, and J. Turlet. 1991. Polarization modulation FT-IR spectroscopy of surfaces and ultra-thin films: experimental procedure and quantitative analysis. *Appl. Spectrosc.* 45:380–389.

Cornut, I., B. Desbat, J. M. Turlet, and J. Dufourcq. 1996. In situ study by polarization modulated Fourier transform infrared spectroscopy of the structure and orientation of lipids and amphipathic peptides at the air-water interface. *Biophys. J.* 70:305–312.

Dluhy, R. A. 1986. Quantitative external reflection infrared spectroscopy of insoluble monolayers spread at the air-water interface. *J. Phys. Chem.* 90:1373–1379.

Ducharme, D., D. Vaknin, M. Paudler, C. Salesse, H. Riegler, and H. Möhwald. 1996. Surface properties of valine-gramicidin A at the air-water interface. *Thin Solid Films.* 284–285:90–93.

Flach, C. R., A. Gericke, and R. Mendelsohn. 1997. Quantitative determination of molecular tilt angles in monomolecular films at the air/water interface: infrared reflection/absorption spectroscopy of behenic acid methyl ester. *J. Phys. Chem. B.* 101:58–65.

Fraser, R. D. B., and T. P. MacRae. 1973. Infrared spectrophotometry. *In* Conformation in Fibrous Proteins and Related Synthetic Polypeptides. Academic Press, New York. 95–125.

Gericke, A., C. R. Flach, and R. Mendelsohn. 1997. Structure and orientation of lung surfactant SP-C and L-α-dipalmitoylphosphatidylcholine in aqueous monolayers. *Biophys. J.* 73:492–499.

Ghadiri, M. R., J. R. Granja, and L. K. Buehler. 1994. Artificial transmembrane ion channels from self-assembling peptide nanotubes. *Nature.* 369:301–304.

Golden, W. G. 1985. Fourier transform infrared reflection-absorption spectroscopy. *In* Fourier Transform Infrared Spectroscopy, Vol. 4. J. R. Ferraro and L. J. Basile, editors. Academic Press, New York. 315–344.

Hansen, W. N. 1968. Electric fields produced by the propagation of plane coherent electromagnetic radiation in a stratified medium. *J. Opt. Soc. Am.* 58:380–390.

Hipps, K. W., and G. A. Crosby. 1979. Applications of the photoelastic modulator to polarization spectroscopy. *J. Phys. Chem.* 83:555–562.

Jähnig, F. 1996. What is the surface tension of a lipid bilayer membrane? *Biophys. J.* 71:1348–1349.

Ketchem, R. R., W. Hu, and T. A. Cross. 1993. High-resolution conformation of gramicidin A in a lipid bilayer by solid-state NMR. *Science.* 261:1457–1460.

Ketchem, R. R., B. Roux, and T. A. Cross. 1997. High-resolution polypeptide structure in a lamellar phase lipid environment from solid state NMR derived orientational constraints. *Structure.* 5:1655–1669.

Kim, H. S., J. D. Hartgerink, and M. R. Ghadiri. 1998. Oriented self-assembly of cyclic peptide nanotubes in lipid membranes. *J. Am. Chem. Soc.* 120:4417–4424.

Langs, D. A. 1988. Three-dimensional structure at 0.86 Å of the uncomplexed form of the transmembrane ion channel peptide gramicidin A. *Science.* 241:188–191.

Lu, J. R., and R. K. Thomas. 1998. Neutron reflection from wet interfaces. *J. Chem. Soc. Faraday Trans.* 94:995–1018.

Majewski, J., T. L. Kuhl, K. Kjaer, M. C. Gerstenberg, J. AlsNielsen, J. N. Israelachvili, and G. S. Smith. 1998. X-ray synchrotron study of packing and protrusions of polymer-lipid monolayers at the air-water interface. *J. Am. Chem. Soc.* 120:1469–1473.

Mendelsohn, R., J. W. Brauner, and A. Gericke. 1995. External infrared reflection absorption spectrometry of monolayers at the air-water interface. *Annu. Rev. Phys. Chem.* 46:305–334.

Nabedryk, E., M. P. Gingold, and J. Breton. 1982. Orientation of gramicidin A transmembrane channel. Infrared dichroism study of gramicidin in vesicles. *Biophys. J.* 38:243–249.

Naik, V. M., and S. Krimm. 1986a. Vibrational analysis of the structure of gramicidin A. I. Normal mode analysis. *Biophys. J.* 49:1131–1145.

Naik, V. M., and S. Krimm. 1986b. Vibrational analysis of the structure of gramicidin A. II. Vibrational spectra. *Biophys. J.* 49:1147–1154.

Naumann, C., C. Dietrich, A. Behrisch, T. Bayerl, M. Schleicher, D. Bucknall, and E. Sackmann. 1996. Hisactophilin-mediated binding of actin to lipid lamellae: a neutron reflectivity study of protein membrane coupling. *Biophys. J.* 71:811–823.

Ohta, K., and H. Ishida. 1988. Comparison among several numerical integration methods for Kramers-Kronig transformation. *Appl. Spectrosc.* 42:952–957.

Sarges, R., and B. Witkop. 1965. Gramicidin A. V. The structure of valine- and isoleucine-gramicidin A. *J. Am. Chem. Soc.* 87:2011–2020.

Tuchscherer, G., and M. Mutter. 1995. Templates in protein de novo design. *J. Biotechnol.* 41:197–210.

Urry, D. W. 1971. The gramicidin A transmembrane channel: a proposed π(L,D) helix. *Proc. Natl. Acad. Sci. USA.* 68:672–676.

Wallace, B. A. 1992. Crystallographic studies of a transmembrane ion channel, gramicidin A. *Prog. Biophys. Mol. Biol.* 57:59–69.

Wallace, B. A. 1998. Recent advances in the high resolution structures of bacterial channels: gramicidin A. *J. Struct. Biol.* 121:123–141.

Wallace, B. A., and K. Ravikumar. 1988. The gramicidin pore: Crystal structure of a cesium complex. *Science.* 241:182–187.

Yamamoto, K., and H. Ishida. 1994. Optical theory applied to infrared spectroscopy. *Vibrational Spectrosc.* 8:1–36.